Analysis of an Anomalous Mutant of MutM DNA Glycosylase Leads to New Insights into the Catalytic Mechanism

Kwangho Nam[1], Gregory L. Verdine[1-4,*], and Martin Karplus[1,5,*]

Department of [1]Chemistry and Chemical Biology and [2]Molecular and Cellular Biology, and [3]Stem Cell and Regenerative Biology, Harvard University, Cambridge, Massachusetts 02138, USA, [4]Program in Cancer Chemical Biology, Dana-Farber Cancer Institute, Boston, MA 02115, [5]L'Institut de Science et d'Ingénierie Supramoléculaires (ISIS), Université Louis Pasteur, 8 allée Gaspard Monge, 67000 Strasbourg, France

Supporting Information

System preparation and molecular dynamics simulations

Systems with oxoG or G at the active site of $MutM^{E3Q}$ and $MutM^{WT}$ were setup based on the X-ray crystal LRC4 structure (PDB code: 2F5S)[1,2] for LRC, and systems for the intrahelical conformation were based on the encounter complex 4 (EC4, PDB code: 3GPU)[2] for oxoG and the interrogation complex 4 (IC4, PDB code: 3GPX)[2] for G. The disordered oxoG-capping loop (residues 215~239) in EC4 and IC4 was built by overlaying the protein portion of LRC4 with the corresponding portion of the EC4 and IC4 structures, respectively. The positions of hydrogen atoms were determined using the HBUILD facility in the CHARMM program[3,4] (version c33a2). Protonation states for all ionizable residues were chosen corresponding to pH 7, except that protonation states of histidine residues (on N_ε and N_δ atoms) were determined on the basis of possible hydrogen bond interactions deduced from the crystal structures; cysteine residues of the Zn-fingers were deprotonated to maintain stable interactions with Zn^{2+} ion, and the E3 residue was either protonated (for system E3-COOH) or deprotonated (for

system E3-COO^-). For the DNA duplex, we kept only 11 central nucleotide base pairs surrounding the target base and discarded the remaining part of the DNA in the crystal structures to retain the same number of nucleotides in the intrahelical and extrahelical systems. The total charge of the resulting protein and DNA duplex was neutralized by placing Na^+ ions (12 Na^+ ions for $MutM^{E3Q}$ and E3-COOH $MutM^{WT}$ and 13 Na^+ ions for E3-COO^- $MutM^{WT}$) 4.5 Å away at the bisector of phosphate groups. All crystal waters were included. The resulting systems were further solvated with a box of water molecules of 75 × 60 × 60 $Å^3$, and water molecules within 2.5 Å of any non-hydrogen atoms of the protein, nucleic acids, Na^+ ions, and crystal waters were removed. The final model for LRC4 containing active site oxoG, for example, has 26088 atoms: 5024 protein and DNA atoms, 13 Na^+ ions, and 7017 water molecules. Periodic boundary conditions were used for the entire simulations.

Each system was energy minimized to alleviate high-energy contacts with a succession of restraints by using conjugate gradient energy minimization (a total of 2500 steps) and Adopted Basis Newton-Raphson energy minimization[3] (a total of 2500 steps), the systems were then equilibrated with molecular dynamics simulations for total 1.7 ns. The leapfrog Verlet algorithm[5] was used with a 2 fs integration time step, and SHAKE[6] was applied to bonds involving hydrogens. The temperature was maintained at 298 K by coupling to an external thermal bath[7], and the volume of system was held constant (NVT condition). The protein, nucleic acids, and ions were represented with the all-atom CHARMM 27 force fields[8-10]; the TIP3P model[11] was used for the water molecules. For the protein backbone dihedral angles, we applied the CMAP correction[12]. The force field parameters for oxoG are the same as presented previously[2]. For electrostatics, the particle mesh Ewald (PME) summation method[13] was used throughout all MD simulations: the calculations used the Ewald κ value of 0.340 $Å^{-1}$ and the approximate grid spacing of 1.0 Å (80×60×60 FFT grid). The real space terms in the PME method were evaluated with a cutoff distance of 9.0 Å. The van der Waals interactions were also evaluated with the same cutoff distance, but were smoothly turned off at the cutoff distance (with SHIFt function).

Potential of mean force calculations

The base extrusion pathway for oxoG was generated by carrying out targeted molecular dynamics (TMD) simulations[2,14-17]. The base extrusion, which is defined as q_{ext} (Fig. S2A), and rotation, which is defined as q_{rotat} (Fig. S2B), were simulated by employing what is often called a steered molecular dynamics algorithm, as introduced by Paci and Karplus[16] and Hut et al.[15]. At the same time, we also applied the restricted-perturbation TMD (RP-TMD)[17] perturbation method on selected atoms at the protein-DNA interface to introduce the conformational change that occurs during the base extrusion process; see reference 2 for details. The important aspects of choosing the parameters and performing the simulations have been described previously[2]. During TMD simulations, the coordinates and velocities were saved every 10ps for the umbrella sampling[18] free energy simulations. Along the base extrusion pathway obtained from the TMD simulations, two-dimensional umbrella sampling free energy simulations[18] were performed with q_{ext} and q_{rotat} (Figs. S2A and S2B) as the progress coordinates. Each umbrella sampling window was separated by 5° from the neighboring windows and was run for 50 ps with a force constant of 0.05 kcal/mol-degree^2 for each progress coordinate. Thus, the total simulation time for MutM^{E3Q} was 36 ns for oxoG and 39 ns for G, for MutM^{WT} with E3-COO$^-$ was 35 ns for oxoG and 39 ns for G, and for MutM^{WT} with E3-COOH was 35 ns for oxoG and 41 ns for G, respectively. The potentials of mean force (pmfs) were computed using the weighted histogram analysis method[19,20]. To test the convergence of the computed pmf values, the umbrella sampling free energy simulations were extended by 50 ps for the extrusion of oxoG by E3-COO$^-$ MutM^{WT} and the computed free energy values were different approximately by 1.8 kcal/mol from the values shown in Fig 3.

Thermodynamic cycle for E3Q mutation and E3 protonation

To do comparison calculations to check the pmf results, thermodynamic cycles were exploited (Schemes S1 and S2). For example, the following free energy equality was applied for the E3Q mutation (see Scheme S1),

$$\Delta\Delta G_{EC\to LRC}^{E3\to Q3} = \Delta G_{LRC}^{E3\to Q3} - \Delta G_{EC}^{E3\to Q3} = \Delta G_{EC\to LRC}^{Q3} - \Delta G_{EC\to LRC}^{E3} \quad (1)$$

where the horizontal free energy changes going from EC to LRC ($\Delta G_{EC\to LRC}$) are the values from the pmf simulations for E3-COO$^-$ and Q3, and the vertical free energy changes going from E3 to Q3 ($\Delta G^{E3\to Q3}$) were computed by carrying out alchemical free energy simulations using λ-dynamics-based thermodynamic integration (TI)[21,22], in which E3 is alchemically mutated to Q3 during the simulation (see below). The quantity $\Delta\Delta G_{EC\to LRC}^{E3\to Q3}$, for example, represents the relative preference of the E3Q mutation when going from EC to LRC. The results are summarized in Table S1 for the E3Q mutation and Table S2 for the protonation of the E3 residue.

The λ-dynamics alchemical mutation simulations

In the λ-dynamics (λ-D) free energy simulations to alchemically mutate the deprotonated E3 side chain to Q3 or protonated E3, the extended Hamiltonian algorithm[22] is used to propagate the λ-particle in the MD simulations. The extended Hamiltonian is defined as,

$$H_{extended}(\lambda) = \lambda H(\lambda = 1) + (1-\lambda)H(\lambda = 0) + \frac{m_\lambda}{2}\dot{\theta}^2 + U_{bias}(\lambda) \quad (1)$$

where $H(\lambda = x)$ is the Hamiltonian for $\lambda = x$, in which x is 0 for deprotonated E3 and 1 for Q3 or protonated E3, respectively, m_λ is the mass for the extended λ particle, and $U_{bias}(\lambda)$ is the λ-dependent umbrella potential. The λ value is defined as

$$\lambda = \mathbf{sin}^2(\theta) \quad (2)$$

where the coordinate, θ, is the variable that is propagated in the MD simulations[23]. In the MD simulations, the temperature of the extended particle was kept at the target temperature by connecting a Nose-Hoover chain of thermostat[24]. In the simulations mutating E3 to Q3 or protonated E3, the total charge of the system changes along with the changes in λ values, and we have applied the background charge correction[25] for the non-zero total charge in the Ewald summation. A total 19 windows covered λ value from 0 to 1; for each window, a total of 300~400 ps MD simulations were carried out to sample the

configuration space. However, the computed values from the TI simulations include the contributions from the internal energies and vibrations of E and Q side chains. To correct for these contributions, we have run additional λ-D simulations for the alchemical mutation of E to Q or protonated E side chain in the gas phase (298 K) and subtracted the computed free energy differences in the gas phase (-32.6 kcal/mol for the E3Q mutation and -23.3 kcal/mol for the protonation of E) from the corresponding free energies for the enzyme-DNA complexes. The values in Tables S1 and S2 are those corrected values.

Calculation of pKa of E3: Poission-Boltzmann and λ-dynamics free energy calculations

The pmf profiles for E3-COOH and E3-COO^- cannot be compared directly; the zero of the pmf for E3-COOH differs from that for E3-COO^- by the free energy required to protonate E3 in a given state, and so a correction has to be introduced. To do so, the pKa value of E3 was computed as the sum of the pKa shift in the intrahelical state (IS) and the experimental pKa value of a Glu (E) side chain in water, with the following equation,

$$pKa^{E3} = \Delta pKa^{E3}_{calc} + pKa^{E}_{ex.sol'n} \quad (2)$$

where ΔpKa^{E3}_{calc} is the computed pKa shift in IS and $pKa^{E}_{ex.sol'n}$ is the experimental pKa of Glu side chain in water (that is 4.1[26]). The ΔpKa^{E3}_{calc} value was computed from the difference of free energy to protonate E3 in IS and in water;

$$\Delta pKa^{E3}_{calc} = -\frac{1}{2.303RT}\left(\Delta G^{E3^-\rightarrow E3H}_{IS} - \Delta G^{E3^-\rightarrow E3H}_{water}\right) \quad (3)$$

where R and T are the gas constant and temperature, respectively, and $\Delta G^{E3^-\rightarrow E3H}_{IS}$ and $\Delta G^{E3^-\rightarrow E3H}_{water}$ are the calculated free energy difference between E3-COOH and E3-COO^- in IS and in water, respectively. Each free energy change was computed by performing alchemical λ-dynamics simulations, in which deprotonated E3 is alchemically mutated to the protonated E3. We have performed the simulations for both oxoG and G: the computed pKa shift (ΔpKa^{E3}_{calc}) is -1.6±1.4 pH unit for oxoG and -1.6±1.0 pH unit for G, respectively. By taking into account the pKa of Glu side chain in water, the pKa value of E3 side

chain in IS is estimated to be 2.5 for both oxoG and G, and therefore, the free energy to protonate E3 at neutral pH is 6.1 kcal/mol. This is added to the pmf profile for E3-COOH as is shown in Figs. 3 and S4, in which the profiles for E3-COO^- are the same as those reported previously[2], and the pmfs for E3-COOH are obtained by using the method described previously[2] for E3-COO^- (also see the "Potential of mean force simulations" section).

To complement the results from λ-D pKa shift calculation, we performed Poisson-Boltzmann calculations[27,28] for oxoG in its intrahelical encounter configuration; the resulting pKa shift value is -1.1 pH units, in approximate agreement with the value from the λ-D simulations (-1.6 pH units). The calculations were based on the X-ray crystal structure for EC4 after minimizations to alleviate high-energy contacts. The Possion-Boltzmann equation was solved by using the finite difference PBEQ solver available in the CHARMM program. Dielectric constants of 80.0 and 20.0 were assigned for water and the protein-DNA system, respectively. A probe radius of 1.4 Å for water was used to generate the solvent-accessible surface. All atomic charges were derived from CHARMM force fields, and all atomic radii were scaled as suggested by Roux and co-workers[29,30]. The ionic salt concentration was set to 0.1 M and a zero ion exclusion radius was used (a 2.0 Å ion exclusion radius was also tested, but it has only a marginal effect on the computed pKa shift). The electrostatic free energy was determined in two steps: (1) the initial calculation was carried out with a coarse grid spacing (0.5 Å) for a 132.0 × 132.0 × 132.0 $Å^3$ cubic box, and (2) the final calculation was carried out with a finer grid spacing (0.25 Å) for a 66.0 × 66.0 × 66.0 $Å^3$ cubic box, in which the boundary potential was interpolated from the potential calculated from the first step. The center of the cubic box was at the E3 residue. The electrostatic potential energy was evaluated for the deprotonated and protonated E3 side chain, respectively. The same calculations were repeated for the E3 side chain in aqueous solution to compute the pKa shift of E3 in EC4, relative to solution.

References

(1) Banerjee, A.; Santos, W. L.; Verdine, G. L. *Science* **2006**, *311*, 1153.
(2) Qi, Y.; Spong, M.; Nam, K.; Banerjee, A.; Jiralerspong, S.; Karplus, M.; Verdine, G. L. **2008**, *submitted*.
(3) Brooks, B. R.; Bruccoleri, R. E.; Olafson, B. D.; States, D. J.; Swaminathan, S.; Karplus, M. *J. Comput. Chem.* **1983**, *4*, 187.
(4) Brooks, B. R.; Brooks, C. L.; MacKerell, A. D., Jr.; Nilsson, L.; Petrella, R. J.; Roux, B.; Won, Y.; Archontis, G.; Bartels, C.; Boresch, S.; Catflisch, A.; Caves, L.; Cui, Q.; Dinner, A. R.; Feig, M.; Fischer, S.; Gao, J.; Hodoscek, M.; Im, W.; Kuczera, K.; Lazaridis, T.; Ma, J.; Ovchinnikov, V.; Paci, E.; Pastor, R. W.; Post, C. B.; Pu, J. Z.; Schaefer, M.; Tidor, B.; Venable, R. M.; Woodcock, H. L.; Wu, X.; Yang, W.; York, D. M.; Karplus, M. *J. Comput. Chem.* **2009**, *30*, 1545.
(5) Allen, M. P.; Tildesley, D. J. *Computer Simulation of Liquids*; Oxford University Press, 1987.
(6) Ryckaert, J. P.; Ciccotti, G.; Berendsen, H. J. C. *J. Comput. Phys.* **1977**, *23*, 327.
(7) Berendsen, H. J. C.; Postma, J. P. M.; Van Gunsteren, W. F.; DiNola, A.; Haak, J. R. *J. Chem. Phys.* **1984**, *81*, 3684.
(8) MacKerell, A. D., Jr.; Bashford, D.; Bellott, M.; Dunbrack, R. L.; Evanseck, J. D.; Field, M. J.; Fischer, S.; Gao, J.; Guo, H.; Ha, S.; Joseph-McCarthy, D.; Kuchnir, L.; Kuczera, K.; Lau, F. T. K.; Mattos, C.; Michnick, S.; Ngo, T.; Nguyen, D. T.; Prodhom, B.; Reiher, W. E., III; Roux, B.; Schlenkrich, M.; Smith, J. C.; Stote, R.; Straub, J.; Watanabe, M.; Wiorkiewicz-Kuczera, J.; Yin, D.; Karplus, M. *J. Phys. Chem. B* **1998**, *102*, 3586.
(9) Foloppe, N.; Mackerell, A. D. *J. Comput. Chem.* **2000**, *21*, 86.
(10) Mackerell, A. D.; Banavali, N. K. *J. Comput. Chem.* **2000**, *21*, 105.
(11) Jorgensen, W. L.; Chandrasekhar, J.; Madura, J. D.; Impey, R. W.; Klein, M. L. *J. Chem. Phys.* **1983**, *79*, 926.
(12) MacKerell, A. D., Jr.; Feig, M.; Brooks, C. L., III *J. Am. Chem. Soc.* **2004**, *126*, 698.
(13) Darden, T.; York, D.; Pedersen, L. *J. Chem. Phys.* **1993**, *98*, 10089.
(14) Schlitter, J.; Engels, M.; Krueger, P.; Jacoby, E.; Wollmer, A. *Mol. Simul.* **1993**, *10*, 291.
(15) Hu, J.; Ma, A.; Dinner, A. R. *J. Chem. Phys.* **2006**, *125*, 114101.
(16) Paci, E.; Karplus, M. *J. Mol. Biol.* **1999**, *288*, 441.
(17) van der Vaart, A.; Karplus, M. *J. Chem. Phys.* **2005**, *122*, 114903.
(18) Torrie, G. M., and Valleau, J. P. *J. Comput. Phys.* **1977**, *23*, 187.
(19) Kumar, S.; Bouzida, D.; Swendsen, R. H.; Kollman, P. A.; Rosenberg, J. M. *J. Comput. Chem.* **1992**, *13*, 1011.
(20) Rajamani, R.; Naidoo, K. J.; Gao, J. *J. Comput. Chem.* **2003**, *24*, 1775.
(21) Kollman, P. A. *Chem. Rev.* **1993**, *93*, 2395.
(22) Kong, X.; Brooks, C. L., III *J. Chem. Phys.* **1996**, *105*, 2414.
(23) Lee, M. S.; Salsbury, F. R., Jr.; Brooks, C. L., III *Proteins* **2004**, *56*, 738.
(24) Martyna, G. J.; Klein, M. L.; Tuckerman, M. *J. Chem. Phys.* **1992**, *97*, 2635.
(25) Figueirido, F.; Del Buono, G. S.; Levy, R. M. *J. Chem. Phys.* **1995**, *103*, 6133.
(26) Lelson, D. L.; Cox, M. M. *Lehninger principles of biochemistry*; 3 ed.; W. H. Freeman: New York, 2000.
(27) Klapper, I.; Hagstrom, R.; Fine, R.; Sharp, K.; Honig, B. *Proteins* **1986**, *1*, 47.
(28) Sharp, K. A.; Honig, B. *Annu. Rev. Biophys. Biophys. Chem.* **1990**, *19*, 301.
(29) Nina, M.; Beglov, D.; Roux, B. *J. Phys. Chem. B* **1997**, *101*, 5239-5248.
(30) Banavali, N. K.; Im, W.; Roux, B. *J. Chem. Phys.* **2002**, *117*, 7381-7388.

Table S1. Computed free energies[a] (kcal/mol) for E3Q mutation from λ-dynamics (λ-D) and pmf simulations.

E3→Q3	$\Delta G_{apo}^{E3\to Q3}$ (*apo* MutM[b])	$\Delta G_{IS}^{E3\to Q3}$	$\Delta G_{LRC}^{E3\to Q3}$	$\Delta\Delta G_{apo\to IS}^{E3\to Q3}$	$\Delta\Delta G_{IS\to LRC}^{E3\to Q3}$	
				λ-D[c]	λ-D[c]	pmf[d]
oxoG[e]	83.8±0.5	83.2±0.7	56.7±1.9	-0.6±1.2	-26.5±2.6	-19.9
G[f]		82.5±0.9	61.3±1.5	-1.3±1.3	-21.2±2.4	-21.1

[a] $\Delta G^{E3\to Q3} = G^{Q3} - G^{E3}$, and $\Delta\Delta G_{A\to B}^{E3\to Q3} = \Delta G_{B}^{E3\to Q3} - \Delta G_{A}^{E3\to Q3}$ (for λ-D) $= \Delta G_{A\to B}^{Q3} - \Delta G_{A\to B}^{E3}$ (for pmf), in which, for example, $\Delta\Delta G_{IS\to LRC}^{E3\to Q3}$ represents the change of the free energy of extrusion in the E3Q mutation between the intrahelical state (IS) and the active site bound state (LRC). All $\Delta G^{E3\to Q3}$ values are corrected for the intramolecular contribution obtained from the gas phase for the E and Q residues (see the text in the Supporting Information).

[b] MutM only; the simulations are carried out with the protein portion alone from the EC4 structure.

[c] The values computed from λ-dynamics calculations.

[d] The values computed from pmf simulations (-19.9 = -14.7 – (+5.2) and -21.1 = -12.1 – (+9.0), where -14.7 and -12.1 are the free energy for oxoG or G extrusion by $MutM^{E3Q}$ from the present pmf simulation, respectively, and +5.2 and +9.0 are for oxoG or G extrusion by $MutM^{WT}$ from previous simulations[2], respectively).

[e] Simulations with oxoG.

[f] Simulations with G, in place of oxoG.

Table S2. Computed free energies[a] (kcal/mol) for the protonation of E3 residue from λ-dynamics (λ-D) and pmf simulations.

E3-COO$^-$ (E3$^-$) →E3-COOH(E3H)	$\Delta G_{Water}^{E3^-\rightarrow E3H}$	$\Delta G_{IS}^{E3^-\rightarrow E3H}$	$\Delta G_{LRC}^{E3^-\rightarrow E3H}$	$\Delta\Delta G_{IS\rightarrow LRC}^{E3^-\rightarrow E3H}$	
				λ-D[b]	pmf[c]
oxoG[d]	89.0±0.2	91.2±1.7	67.5±0.2	-23.7±1.9	-19.0
G[e]		91.3±1.2	74.9±0.6	-16.4±1.8	-14.5

[a] $\Delta G^{E3^-\rightarrow E3H} = G^{E3-COOH} - G^{E3-COO^-}$, and $\Delta\Delta G_{A\rightarrow B}^{E3^-\rightarrow E3H} = \Delta G_B^{E3^-\rightarrow E3H} - \Delta G_A^{E3^-\rightarrow E3H}$ (for λ-D) $= \Delta G_{A\rightarrow B}^{E3-COOH} - \Delta G_{A\rightarrow B}^{E3-COO^-}$ (for pmf), in which, for example, $\Delta\Delta G_{IS\rightarrow LRC}^{E3^-\rightarrow E3H}$ represents the change of the free energy of extrusion in the protonation of E3 residue. $\Delta G_{Water}^{E3^-\rightarrow E3H}$ is the free energy change of the protonation of E3 side chain in aqueous solution. All $\Delta G^{E3^-\rightarrow E3H}$ values are corrected for the intramolecular contribution obtained from the gas phase for the E-COO$^-$ and E-COOH residues.

[b] The values computed from λ-dynamics calculations.

[c] The values computed from pmf simulations (-19.0 = -13.8 – (+5.2) and -14.5 = -5.5 – (+9.0), where -13.8 and -5.5 are the free energy for base extrusion by MutM^{WT} with E3-COOH for oxoG and G, respectively, from the present pmf simulation, and +5.2 and +9.0 are the same free energy by MutM^{WT} with E3-COO$^-$ for oxoG and G, respectively, from previous simulations[2]).

[d] Simulations with oxoG.

[e] Simulations with G.

Scheme S1. Thermodynamic cycle for computation of the free energy difference between oxoG extrusion from $MutM^{WT}$ and $MutM^{E3Q}$.

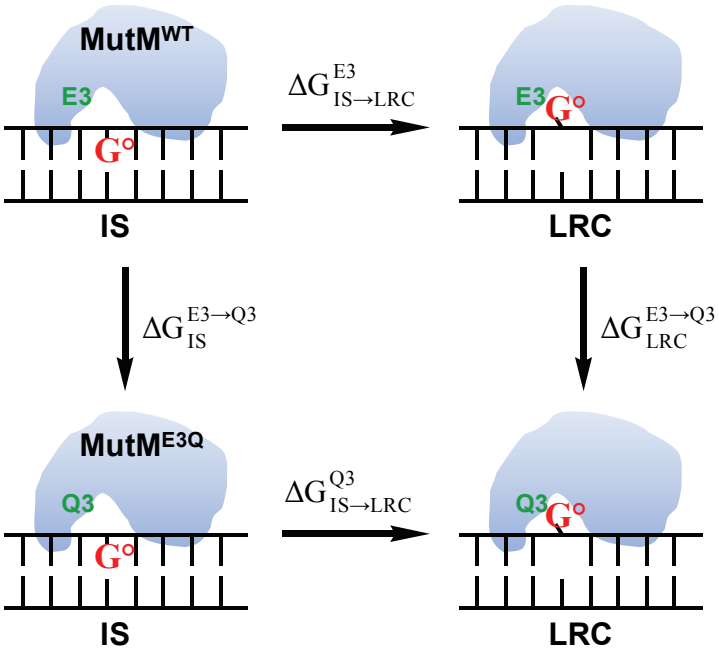

Scheme S2. Thermodynamic cycle representing the relationship between the free energy profiles of oxoG extrusion by $MutM^{WT}$ with E3-COOH and $E3\text{-}COO^-$.

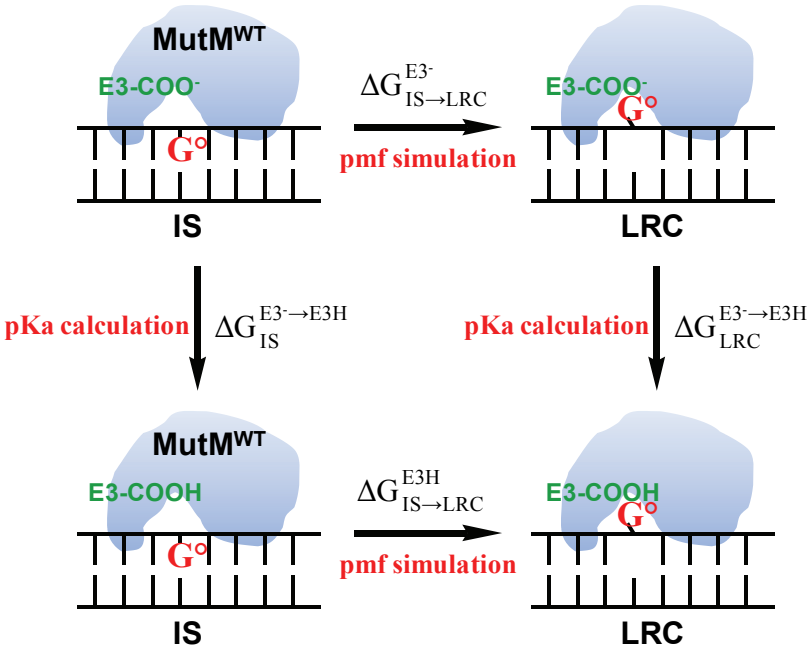

Figure S1. Potentials of mean force along the progress variable r ($r = q_{rotat} - q_{ext}$) for the (A) oxoG and (B) G extrusion by MutM^{E3Q} (green) and MutM^{WT} with a deprotonated E3 residue (blue). The indicated points correspond to the points labeled in Fig. 2, and the free energy value at the intrahelical state (IS) is set to zero for each profile.

(A)

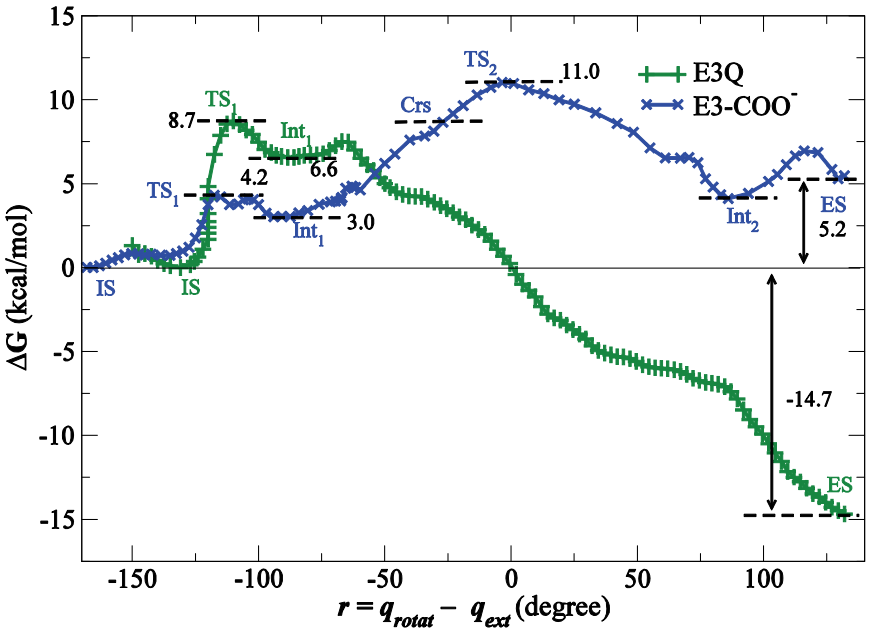

Figure S1.

(B)

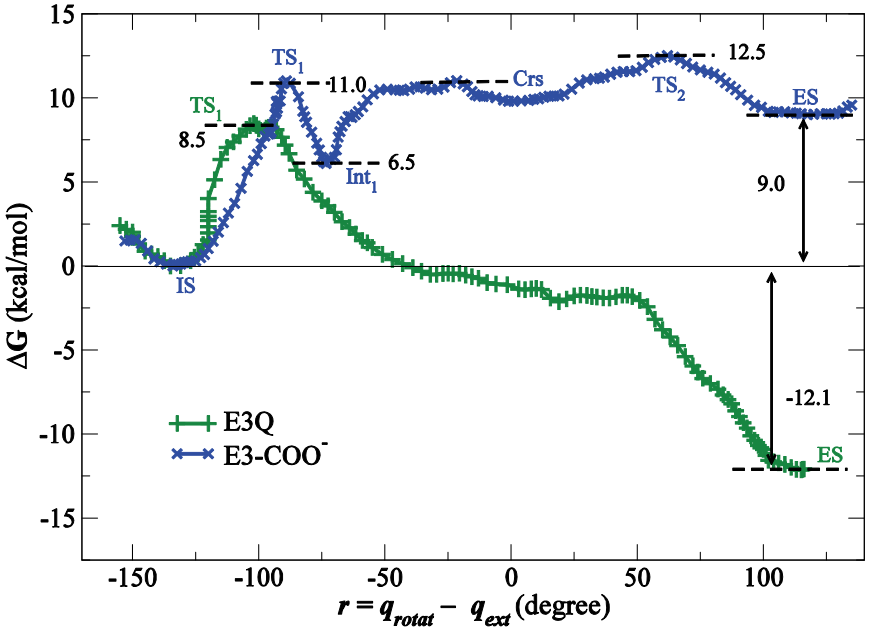
15
10
5
0
-5
-10
-15
ΔG (kcal/mol)
-150
-100
-50
0
50
100
r = q_rotat − q_ext (degree)
TS1
11.0
TS1
8.5
Int1
6.5
IS
Crs
TS2
12.5
ES
9.0
-12.1
ES
E3Q
E3-COO-

Figure S2. Definition of the center of mass pseudo-dihedral angles for (a) the base extrusion, q_{ext} and (b) the base rotation, q_{rotat} .

(a)

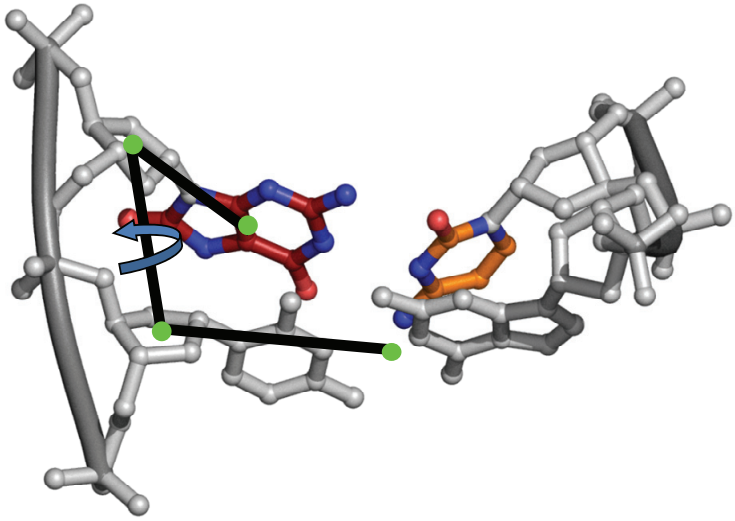

Figure S2 (b).

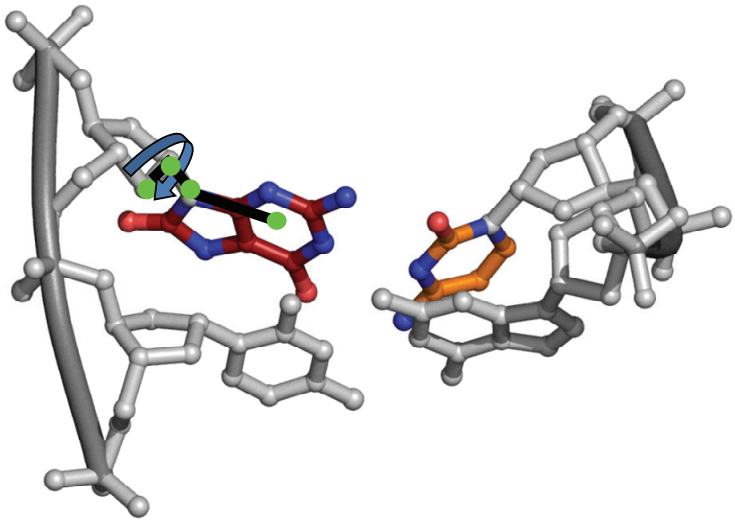

Figure S3. Computed contribution of each (a) amino acid residue and (b) nucleotide on $\Delta G_{IS}^{E3\rightarrow Q3}$ (EC4) and $\Delta G_{LRC}^{E3\rightarrow Q3}$ (LRC4). In (a), the plot for LRC3 is shifted to the right by 1 for a clear view, and in (b), the oxoG nucleotide is located in DNA strand 2 (sequence number 25).

(a)

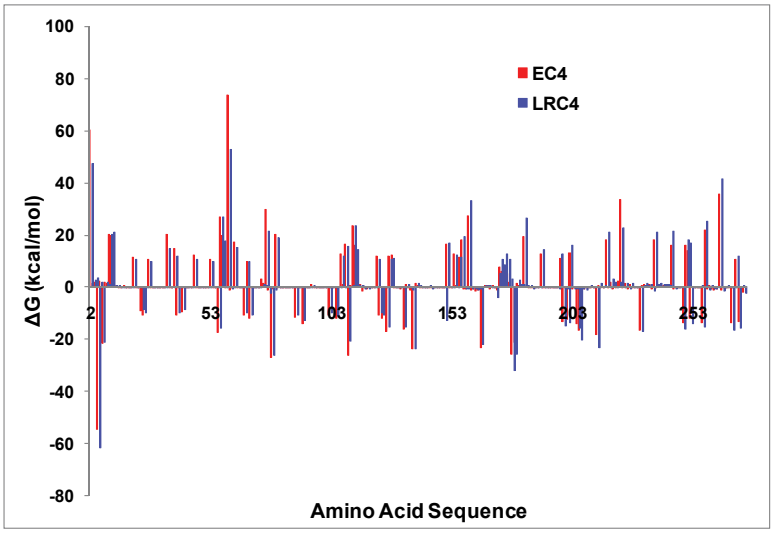

(b)

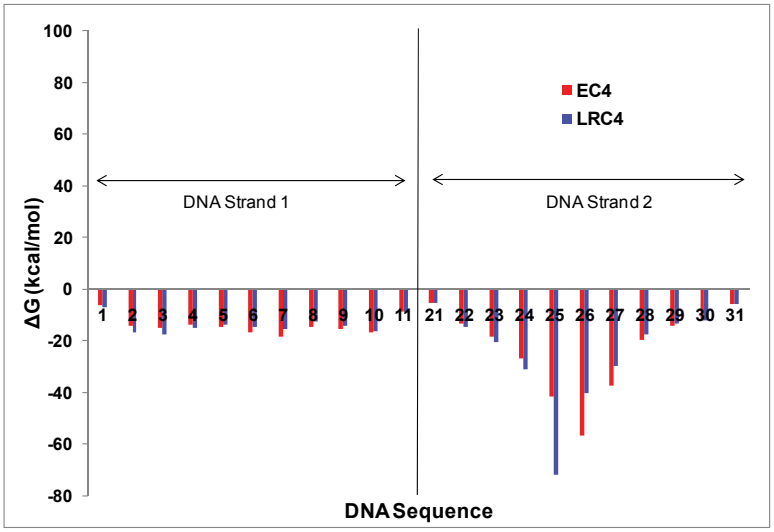

Figure S4. Potentials of mean force along a progress variable (r) equal to the difference q_{rotat} and q_{ext} for G extrusion by MutM^{WT} with a protonated (red) or deprotonated (blue) E3 residue. The profiles for E3-COOH are shifted upward by 6.1 kcal/mol, the free energy required to protonate E3 residue at pH 7 (see Supporting Information). Indicated point correspond to points labeled in Fig. 2 and Fig. S5. The zero of free energy is that of the intrahelical state (IS).

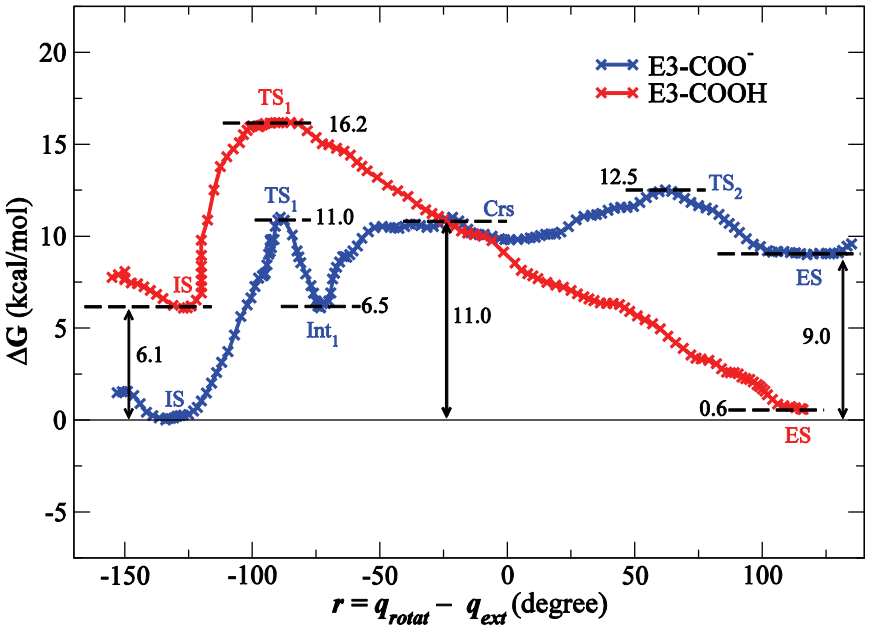

Figure S5. Computed potential of mean force for oxoG extrusion by MutM^{WT} for E3-COOH. The unit for dihedral angles is degree and for free energy is kcal/mol. The minimum free energy path is also indicated as black dots.